ORIGINAL PAPER

A rock mechanics calculation model for identifying bed separation position and analyzing overburden breakage in mining

Jiang-hui He[1] · Wen-ping Li[1] · Wei Qiao[1]

Abstract

During coal seam mining, the overlying rock can deform, break, and produce a large number of fractures, including horizontal and vertical fractures; the horizontal fractures are also known as bed separation. A bed separation water disaster (BSWD) is a destructive release of roof water, and preventing BSWDs requires accurate location of bed separation positions. A calculation model for overburden deformation and fracture analysis during mining is therefore needed. First, the deformation and breakage area of overlying rock above an active mining face were reduced to a triangular overburden deformation area (TODA), based on the results of similar material simulation experiments. Second, the hierarchy comparison merging method (HCMM) was proposed to analyze the combination and separation of rock layers in the overlying strata. The triangular calculation model (TCM), which can be used to identify bed separation locations and analyze overlying strata breakage, was then obtained by combining TODA with HCMM, and the discriminant principle and related calculation formulas of the model were given. Finally, the model was applied and validated using a mining case, showing that the TCM is a practical tool for analyzing bed separation position and overburden breakage during mining.

Introduction

China continues to undertake large-scale coal exploitation and thus faces an ongoing risk of coal seam roof water disasters. A bed separation water disaster (BSWD) is a relatively recent type of roof water disaster. It has resulted in several major underground disasters during mining operations. For example, on May 21, 2005, a BSWD accident occurred at the Haizi coal mine in Huaibei, killing five people. On July 18, 2011, the mixture of water and gas ejected from the #10414-2 gas drainage hole of the 10414 mining face in Yangliu coal mine was initiated by bed separations in overlying rock (Wang 2013; Xu et al. 2014). On April 25, 2016, 11 people died in a BSWD accident at Zhaojin coal mine in Tongchuan. Accurately

locating potential bed separation positions is essential to preventing this type of water disaster. Bed separation is a layered cavity formed during the deformation and failure of overlying rock. Therefore, in order to prevent BSWD, it is necessary to analyze the deformation and failure processes of overlying strata during mining.

Bed separation occurs after the overburden is disturbed by mining, so overburden deformation and failure after mining should be analyzed. Based on overburden rock deformation characteristics, Chinese researcher Liu (1981) stated that the overlying rock layer, from bottom to top, is comprised of a caving zone, fracture zone, and curved subsidence zone. The caving zone and the fracture zone can drain water from overlying aquifers to a mine, so the two zones are often referred to as the flowing water fracture zone (FFZ). Liu et al. (2015) used numerical simulation to show that the height of the FFZ increases with both the mining face length and mining thickness. In general, because bed separation cavity with an intact sealing property should be located above the FFZ, it is necessary to calculate the height of the FFZ before identifying bed separation positions. Wei et al. (2017) and Qiao et al. (2017) found that FFZ height in western China coal mines

---

Responsible Editor: Amjad Kallel

✉ Jiang-hui He
hjh@cumt.edu.cn

1 School of Resources and Geosciences, China University of Mining and Technology, Xuzhou 221116, China

was positively correlated to coal seam thickness. Thus, the ratio of FFZ height to mining thickness becomes a key parameter that can be used to calculate FFZ height in practice. Specifically, pressure arch theory, key strata theory, composite beam theory, stochastic medium theory, numerical simulation, similar material simulation, field measurements, and a combination of various research methods have been adopted by many scholars when identifying the bed separation position.

Theoretical analysis is often used to study overburden deformation and failure. Peng (1984) used pressure arch theory to explain the phenomenon that rock above the goaf is in a state of pressure release involving bed separation. Bieniawski (1990) stated that bed separation could develop in fracture zones, and Gao (1996) and Gao et al. (2001) defined the rock layer located above the fracture zone and at the bottom of the curved subsidence zone as the bed separation zone. Palchik (2003) divided the fracture zone that forms above the caved zone into three parts: rock blocks, through-going vertical fractures, and horizontal fractures caused by bedding layer separation. Furthermore, Qian and Shi (2003), Qian et al. (2003), and Xu et al. (2004) proposed key stratum theory and showed that bed separation mainly occurs beneath the key stratum. Furthermore, Yue et al. (2015) and Yan et al. (2016) estimated bed separation position during mining using the composite beams principle. Jiang (1997) and Jiang and Xu (1997) provided a theoretical discussion of the distribution regularities and causal mechanisms of bed separation within the overburden during mining. Wang et al. (1999) demonstrated that the height of the bed separation zone changes as a function of the goaf size under the same geological and mining conditions. These studies showed that macroscopic theoretical analysis can partition the extent of overlying rock deformation, and simple macroscopic mechanical analyses can be conducted. However, a disadvantage of this method is that it is often used when overlying rock deformation and damage are finished and the overlying rock has been stabilized again after mining completion, so that the rock stratum deformation destruction and force conditions at different excavation distances cannot be obtained. Moreover, general theoretical analysis may not accurately quantify the bed separation position, and there is inevitable deviation of the results caused by the simplification of many conditions.

Simulation experiments, including numerical simulation and similar material simulation, are a convenient way to study overburden deformation and failure . Xu et al. (2015) and Cheng et al. (2017b) analyzed key stratum controls on overburden subsidence through numerical simulations. Xue et al. (2015) determined the pressure relief range through similar material simulation. Meanwhile, Yu (2007) employed a test model to show that the height of the bed separation position is approximately 0.4 to 0.6 times the excavation distance; simulations by Wang et al. (2015) produced similar results.

Zhao et al. (2002) concluded that the maximum height of the bed separation position is approximately 0.43 to 0.67 times the mining depth. The advantage of numerical simulation is that we can conduct complex mechanics calculations using a computer, and the appearance of overlying rock fractures, the deformation state, and the distribution of bed separation at different locations can be presented intuitively. The disadvantages are that details of the computer calculations and whether there were any factors that had not been taken into account may not be known, resulting in phenomena that are not practical or remain undetected. Similar material simulation experiments of mine conditions can be scaled down according to known similarity ratios, so that observations can be made in a laboratory, although it is not possible to ascertain the forces and deformation trends of each rock layer in the model at any given moment. In addition, in many numerical simulation and similar material simulation experiments, model structure is often simplified or idealized, resulting in a deviation between the simulation results and the actual results.

Bed separation observation, including field observation, has also been carried out (Cheng et al. 2017a; Ding et al. 2010; Fan 2014; Kuang et al. 2019; Lu et al. 2016; Palchik 2005; Tan et al. 2013; Wen and Zhang 2006; Xiao et al. 2015; Zhao 2016; Zhao et al. 2008; Zhou 2015b). Borehole observation, including borehole wall imaging and strata subsidence observation, is a common field measurement method. The observation results can directly reflect the distribution of fractures in the overburden and the subsidence difference between different strata. However, borehole observation requires high drilling quality. If the observation hole is disturbed by mining, resulting in hole collapse, blockage, or staggered structure, the observation cannot be carried out. Fiber-Bragg-grating (FBG) monitoring is an emerging means to assess overlying rock layer deformation (Chai et al. 2011, 2015; Zhang et al. 2017; Zhao et al. 2015). The advantage of FBG monitoring is that in situ tests can be carried out at the mining sites, avoiding errors caused by simplified lab conditions. The FBG can be installed in the roof rock of the mining face before mining, and the overlying strata deformation can be monitored by fiber deformation during the subsequent mining process. However, when the fiber is broken at a certain depth, it only reflects the existence of fractures in the buried depth and cannot determine if the fracture orientation is horizontal (i.e., bed separation) or vertical (or near-vertical). In short, FBG monitoring can only monitor the presence of fractures, but cannot identify the fracture types. In addition, the fiber is broken when the fracture is formed so that any subsequent closing of fractures due to compaction can no longer be monitored.

Using a combination of several methods to carry out research can produce richer and more accurate information. Su (2001) and Su et al. (2003) studied deformation mechanics of overlying rock by using numerical simulation, similar material simulation, and theoretical analysis and concluded that the

pressure balance arch inside the overlying rock layer is the precondition for producing bed separation and the position height and span of bed separation is half the excavation distance. Based on key strata theory, stochastic medium theory, and numerical simulation, Wang and Li (2016) and Wang et al. (2016a, 2016b, 2017) proposed a series of void rate distribution models in disturbed strata that showed the fracture ratio in the bed separation zone. Other workers have studied the influence of different factors on bed separation using numerical simulation, similar material simulation, and field measurements (An and Wu 2008; Man 2014; Palchik 2010; Sun 2012; Wu et al. 2012; Yu and Wang 2006; Zhang and Chen 1996; Zhao et al. 1998). Although the use of multiple methods increases the workload, results based on different methods can produce a deeper understanding of the research subject. Therefore, in the field of bed separation, a combination of various research methods is commonly used.

In this paper, a modeling approach was used to predict bed separation position, coal roof collapse, and catastrophic water inflows during underground coal mining. The model evaluates the development of overburden horizontal fractures above the mined area, and the process by which they form, fill with water, and are compressed as part of the evolution of the stress field in the overlying strata as the mining face advances. Theoretical analysis, laboratory studies, and field studies were carried out to establish the model and related formulas. The research results suggest that this model application may be useful in preventing roof collapse, mine flooding, and loss of life.

Determination of the shape of the overburden deformation area

Space-time distribution of bed separation

For any size of goaf, a pressure balance arch develops in the overlying strata. With loss of support, strata within the balance arch can bend and subside under their own weight. Thus, the area within the balance arch is the only area where overburden deformation occurs and bed separation forms, so it can be called the overburden deformation area. The overburden deformation area grows, and the bed separation develops dynamically in both horizontal and vertical directions (Fig. 1).

Triangular deformation area

The actual shape equation of the balanced arch is influenced by many factors, including depth, thickness of mined layer, and lithology, so that its calculation is complex and not easily applied. We considered a similar material simulation of the 21301 mining face of the Cuimu coal mine in Baoji City,

Shaanxi Province, China, to study development of the overburden deformation area during the mining process.

Model design and fabrication

The coal seams mined in the Cuimu coal mine were deposited in the Ordos Basin during the Jurassic. As shown in Fig. 2, mining face 21301 is located in the eastern portion of the mine and is 968-m long, 214-m wide, and 488.61-m deep. The total thickness of the bedrock is 471.22 m, the thickness of loose layer is 17.39 m, and the average thickness at the mining face is 10 m.

The parameter similarity ratio, material ratio, and specific experimental process used have been described in existing literature (Zhou 2015a). The study volume is defined with reference to the engineering geological histogram (Fig. 3) for mining face 21301; its length, width, and height were 500 m, 40 m, and 240 m, respectively. The applied stress from overlying rock was simulated in the model by a compensatory external load. The length, width, and height of the model were 2.5 m, 0.2 m, and 1.2 m, respectively. The strength index was selected as the main similarity index of both the study volume and model, and the converted compensatory external load was 7.48 kN. In addition, based on the division principle of engineering geology, rock layers with similar geological and mechanical properties were merged into a single petrofabric. A diagram of the model layout is shown in Fig. 4; petrofabric divisions and converted factors for the model are shown in Table 1.

In this study, the similar material simulation model was based on the inverse similarity theorem, and the calculated ratios for length similarity, time similarity, stress similarity of rock, and stress similarity of coal were 200, 14, 306, and 182, respectively. In Table 1, the model's parameter values were converted by dividing the prototype's parameter values by the corresponding similarity ratio.

Model mining and experimental results analysis

The excavation process is shown in Fig. 5.

It is found that bed separation and strata bending and fracturing only occurred within the rock layers between the two rock rupture lines (i.e., the oblique purple lines in Fig. 5), where loss of support occurred. The triangular area bounded by the two rock rupture lines and the coal seam roof (cyan horizontal line in Fig. 5) approximates the overburden deformation area. We defined this area as the triangular overburden deformation area (TODA). Yu (2007) showed that the rock breaking angle (i.e., the angle between the rock rupture line and the coal seam roof in Fig. 5) ranged from 55° to 65°; the average is considered 60°. Accordingly, both the existence and the general shape of the overburden deformation area were considered. Computational difficulty was reduced, and operability was enhanced.

Fig. 1 Distribution of the overburden deformation area and bed separation during mining
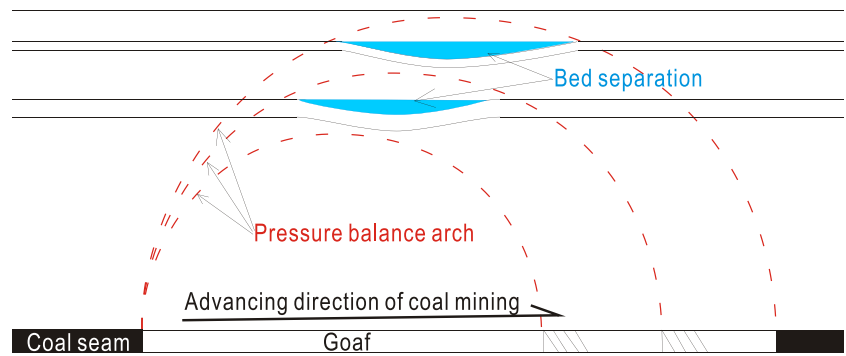

Identification of rock layer contact state

Once the overburden deformation area was determined, the deformation of rock layers within that area is needed to be analyzed. Evaluating the contact relationship between adjacent strata involved ascertaining whether bed separation occurred between adjacent strata; when the adjacent strata were not in contact, bed separation was deemed to have occurred between the two layers. He et al. (2018) proposed the hierarchy comparison merging method (HCMM) to identify the contact state of the rock layer, which was used in this study.

Identification principle

A composite beam is formed by *n* layers that can produce synchronized bending deformation. Because a large bed separation that can accumulate water is located only in the middle of the suspended rock beam span, deformational analysis only needs to be performed for that part of the rock beam. (Below, by "curvature," we refer only to the curvature of a rock beam in the middle of the suspended span.) HCMM can merge adjacent rock beams for which the upper beam curvature exceeds that of the lower beam into a larger composite beam by comparing the

Fig. 2 Location of the study area
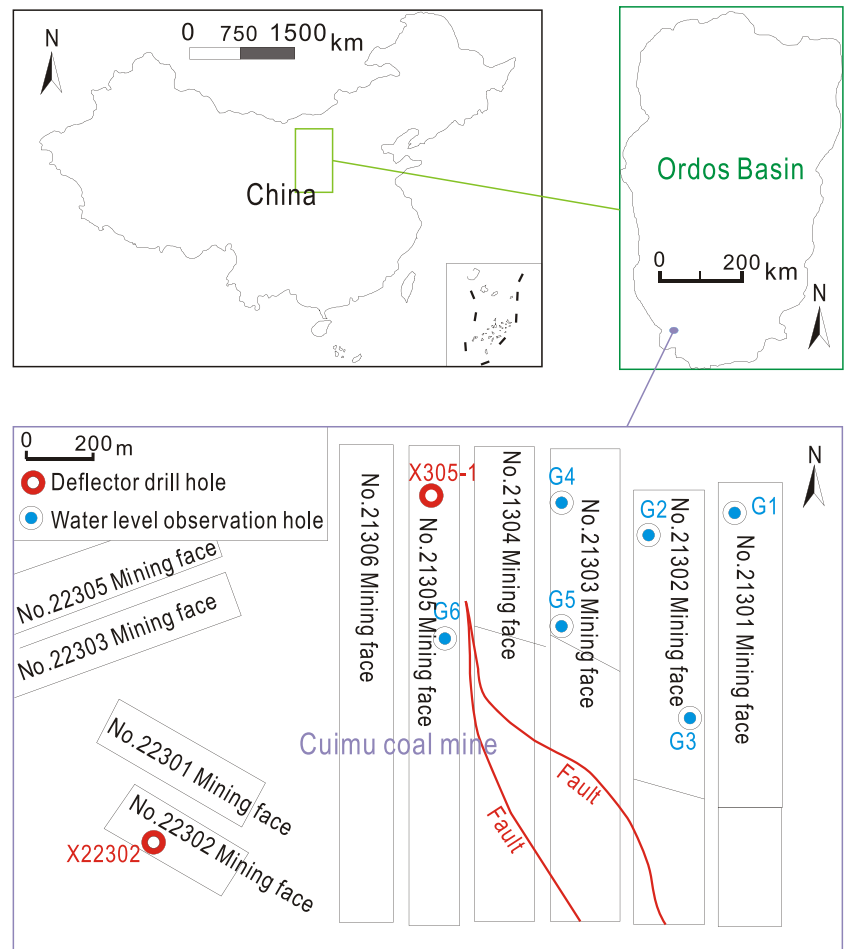
Table 1 Conversion of rock mass index

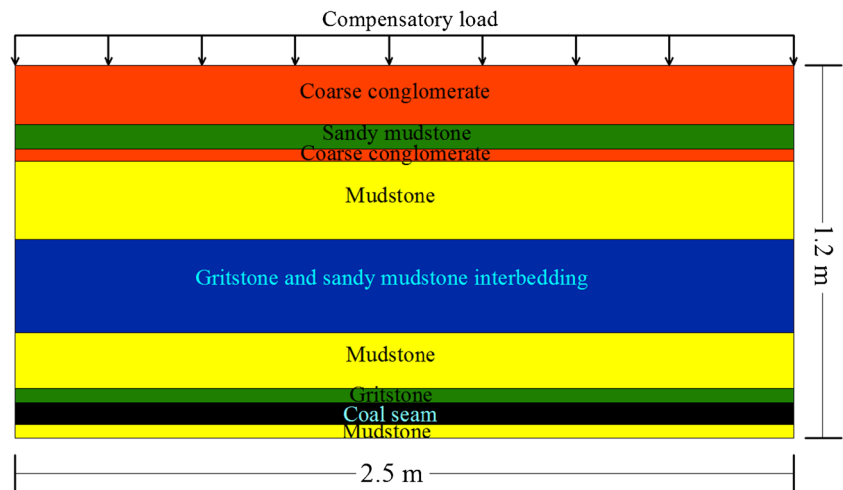| No.	Lithology	Original rock parameters			Converted model parameters		
		Average thickness (m)	Compressive strength (MPa)	Tensile strength (MPa)	Thickness (mm)	Compressive strength (kPa)	Tensile strength (kPa)
1	Coarse conglomerate	42	45.88	1.45	210	149.94	4.74
2	Sandy mudstone	16	26.54	0.98	80	86.73	3.21
3	Coarse conglomerate	8	45.88	1.45	40	149.94	4.74
4	Mudstone	50	21.90	0.88	250	71.57	2.88
5	Gritstone and sandy mudstone interbedding	60	4.3	0.24	300	14.05	0.78
6	Mudstone	36	21.90	0.88	180	71.57	2.88
7	Gritstone	9	30.32	1.25	45	99.08	4.08
8	Coal seam	10	11.15	0.29	50	61.26	1.59
9	Mudstone	9	21.90	0.88	45	71.57	2.88

curvature of adjacent rock beams. When all adjacent rock beams and composite beams are merged, the merger is completed, and the real contact state between each rock layer can be shown. Bed separation occurs between adjacent composite beams for which the curvature of the upper composite beam is less than the curvature of the lower composite beam.

Fig. 3 Schematic geologic column of mining face 21301

No.	Legend	Lithology	Average thickness (m)	Compressive strength (Mpa)	Tensile strength (Mpa)	Density (g/cm³)
1		Loess	18			
2		Sandy mudstone	44	11.9	0.52	2.46
3		Pebbly sandstone	28	18.5	0.56	2.25
4		Coarse conglomerate	109	58.7	1.68	2.48
5		Medium sandstone	4	13.3	0.42	2.31
6		Coarse conglomerate	36	33	1.23	2.32
7		Gritstone	31	4.9	0.24	2.24
8		Coarse conglomerate	28	45.88	1.45	2.48
9		Medium sandstone	12	13.3	0.42	2.31
10		Sandy mudstone	4	30.3	1.2	2.34
11		Coarse conglomerate	4	36.8	1.35	2.58
12		Gritstone	6	3.9	0.24	2.21
13		Mudstone	12	23.9	0.98	2.21
14		Gritstone	6	4	0.24	2.21
15		Mudstone	32	21.5	0.88	2.21
16		Gritstone	6	4.1	0.24	2.2
17		Sandy mudstone	46	4.3	0.24	2.25
18		Gritstone	7	4.1	0.24	2.21
19		Mudstone	22	23.9	0.98	2.41
20		Fine sandstone	4	23.9	0.98	2.39
21		Mudstone	16	21.5	0.88	2.33
22		Gritstone	7	13.6	0.6	2.34
23		Coal seam	10	11.15	0.29	1.37
24		Mudstone	6	21.9	0.88	2.49

Fig. 4 Schematic diagram of model layout

Compensatory load

Coarse conglomerate

Sandy mudstone

Coarse conglomerate

Mudstone

Gritstone and sandy mudstone interbedding

Mudstone

Gritstone

Coal seam

Mudstone

1.2 m

2.5 m

For example, assuming that there are 15 layers of rock beams above the goaf, the curvature of each rock beam under the action of its own weight is recorded in Hierarchy I in Fig. 6. After four mergers, the merger is over and four composite beams, and three bed separations are formed (Fig. 6).

Related formulas

Calculation of rock beam curvature

As shown in Fig. 7, there are m layers of rock layer above the goaf. The thickness, volume weight, elasticity modulus, moment of lateral section inertia, and uniformly distributed load of self-weight for each beam are, respectively, given by h_i, γ_i, E_i, I_i, and q_i ($i = 1,2,3,\ldots n\ldots,m$). In a composite beam with n layers of rock beams, the bending moment sustained by the ith ($i = 1,2,3,\ldots n$) beam in the middle of its suspended span is $(M_n)_i$. This bending moment causes the beam to experience bending deformation with a curvature of $(C_n)_i$ in the middle of its suspended span. The relationship between $(M_n)_i$ and $(C_n)_i$ can be expressed as follows:

$$(C_n)_i = \frac{(M_n)_i}{E_i I_i} \tag{1}$$

Because n layers of a rock beam can bend synchronously, each individual beam in a composite beam has the same curvature. Thus, the composite beam curvature (C_n) can be replaced by a curvature $(C_n)_i$ ($i = 1, 2, \ldots n$) of any individual beam in the composite beam. That is:

$$(C_n) = (C_n)_1 = (C_n)_2 = \ldots = (C_n)_{n-1} = (C_n)_n \tag{2}$$

When the thickness of the ith ($i = 1,2,3, \ldots n$) beam is h_i and its width is b_i, I_i can be expressed as:

$$I_i = \frac{b_i h_i^3}{12} \quad , (\, i = 1, 2, \ldots \text{n}) \tag{3}$$

When the width of each beam b_i defaults to a unit width, (3) can be simplified as:

$$I_i = \frac{h_i^3}{12} \quad , (\, i = 1, 2, \ldots \text{n}) \tag{4}$$

Value ranges of composite beam curvature

In each hierarchy, for each composite beam with n layers of rock beams that can bend simultaneously, when the deformation of each rock beam is analyzed individually, the curvature C_i($i = 1, 2, \ldots n$) caused only by a beam's self-weight load has the following characteristics:

$$C_1 < C_2 < C_3 < \ldots < C_{n-1} < C_n \tag{5}$$

Each rock beam is supported by the beam immediately below it and bends simultaneously with this adjacent rock beam. A composite beam with n layers of rock beam can thereby be achieved only with the existence of such a curvature size relation. The value ranges of composite beam curvature (C_n) are as follows:

$$C_i\big|_{\text{min}} < (C_n) = (C_n)_1 = (C_n)_2 = \ldots = (C_n)_n < C_i\big|_{\text{max}} \tag{6}$$

Proposal and application of the triangular calculation model

After the preceding analysis and preparation, a triangular calculation model (TCM) to identify the bed separation position

Fig. 5 Similar material simulation experiment on bed separation and roof deformation with changes in excavation distance in mining face 21301: (**a**) Footage of 120 m; (**b**) Footage of 270 m; (**c**) Footage of 400 m
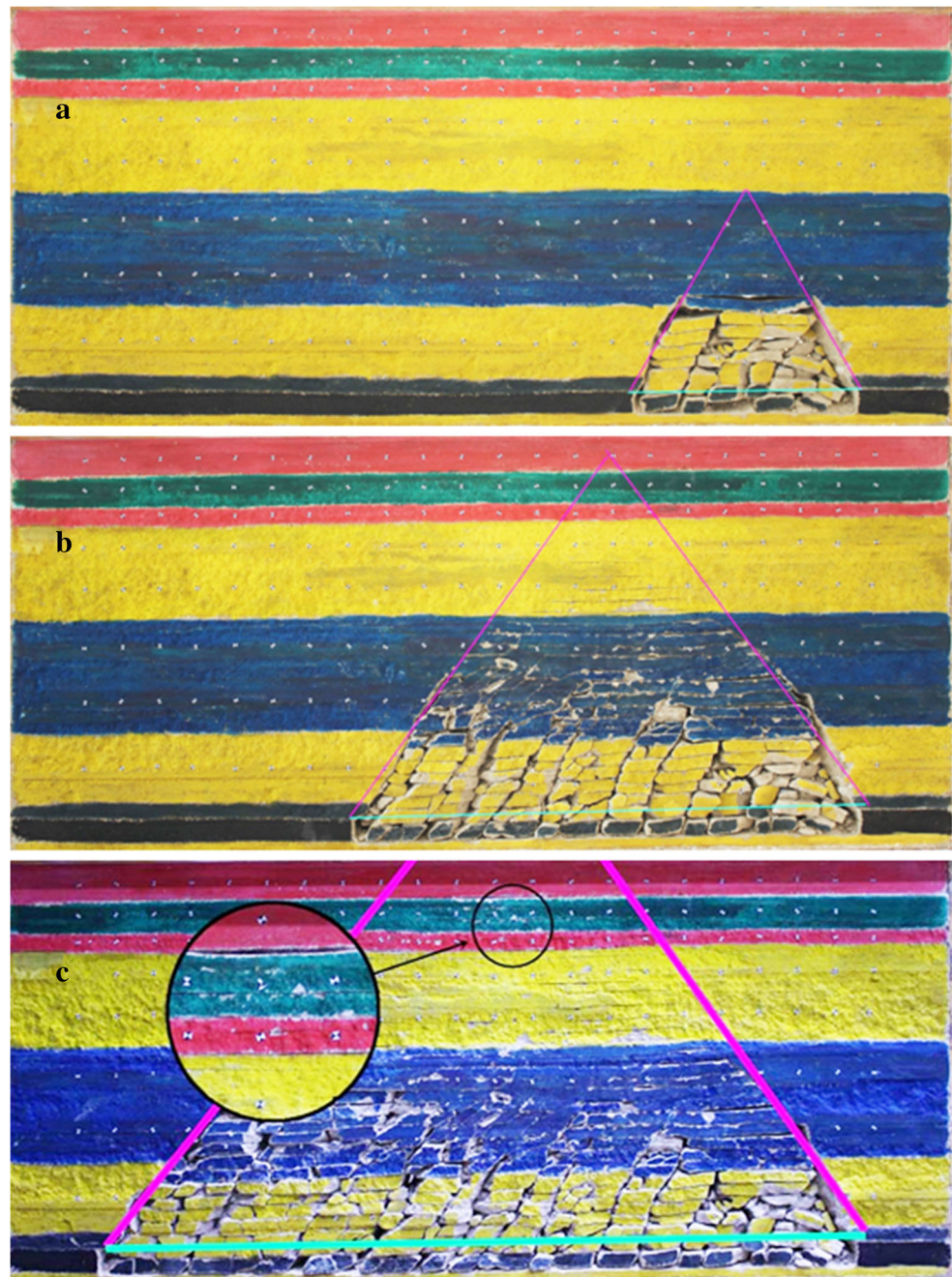
and analyze overlying strata breakage was obtained by combining the TODA with HCMM.

Instructions for use

The application of HCMM in the TODA was consistent with the main identification principle of HCMM described in Identification of rock layer contact state, with the exception of the following:

(1) Not all overlying strata were in involved in the calculation, comparison, and merging. Only the strata within the TODA are needed to be calculated and analyzed.

(2) The suspended span length of each rock layer involved in the calculation was different. The length of the suspended span decreased from bottom to top.

(3) The calculation process was performed under the condition that all strata being computed were not broken, i.e., all strata were intact. Because the

No.	Curvature $(C_n)_i$ $(1\times10^{-6}\cdot m^{-1})$				
	Hierarchy I	Hierarchy II	Hierarchy III	Hierarchy IV	Hierarchy V
15	0.86	Composite II-I 0.15	Composite III-F 0.13	Composite IV-E 0.13	Composite V-D 0.13
14	0.57				
13	0.07				
12	5.60	Composite II-H 0.10			Bed separation V-③
11	0.09				
10	0.62	Composite II-G 0.62	Composite III-E 0.56	Composite IV-D 0.56	Composite V-C 0.56
9	4.00	Composite II-F 0.53			
8	0.41				Bed separation V-②
7	10.25	Composite II-E 10.25	Composite III-D 10.25	Composite IV-C 10.25	Composite V-B 8.90
6	17.60	Composite II-D 16.89	Composite III-C 16.89	Composite IV-B 8.68	
5	15.98				
4	32.77	Composite II-C 32.77	Composite III-B 6.49		
3	33.08	Composite II-B 5.08			
2	3.53				Bed separation V-①
1	30.39	Composite II-A 30.39	Composite III-A 30.39	Composite IV-A 30.39	Composite V-A 30.39
	Goaf				

First merger → Second merger → Third merger → Fourth merger
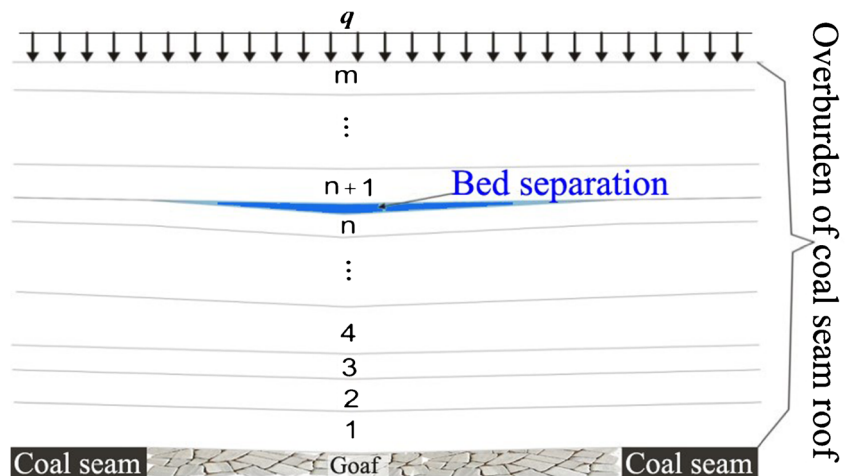
Fig. 6 Schematic diagram of the process of merging rock beams using HCMM

rupture of rock layer proceeded from the bottom to the top, it was only necessary to ensure that the bottom rock layer was not broken. If rock layers in the lower part of the TODA were broken, the calculation included only the unbroken rock layers in the upper part of the TODA.

(4) For the rock layers in the FFZ, both deformation and breaking problems were considered, while only deformation problems needed to be considered for the rock layers in the curved subsidence zone (Fig. 8).

Under certain mining conditions, the maximum height of the FFZ was limited and could be predicted. The hermetic status of bed separation cavities inside the FFZ was destroyed, while bed separation cavities inside the curved subsidence zone remained hermetic and could accumulate water.

TCM and related formulas

The actual load form borne by each rock layer in the TODA varied with the number of rock layers, resulting in a variation in the formulas for corresponding curvature and maximum tensile stress. The classification of the relevant discriminant formulas for a composite beam containing n layers of rock beams is described below:

$n = 1$

As shown in Fig. 9a, the rock layers in the TODA consist of the first and second layers; however, only the first layer satisfied the condition of having its whole thickness within the TODA. The shape of the suspended span of the first layer rock beam was a trapezoid (including the red and purple parts). To simplify the calculation, the suspended span was

Fig. 7 Definition of terms used for location identification of bed separation

Fig. 8 Overburden deformation-
zone divisions after mining
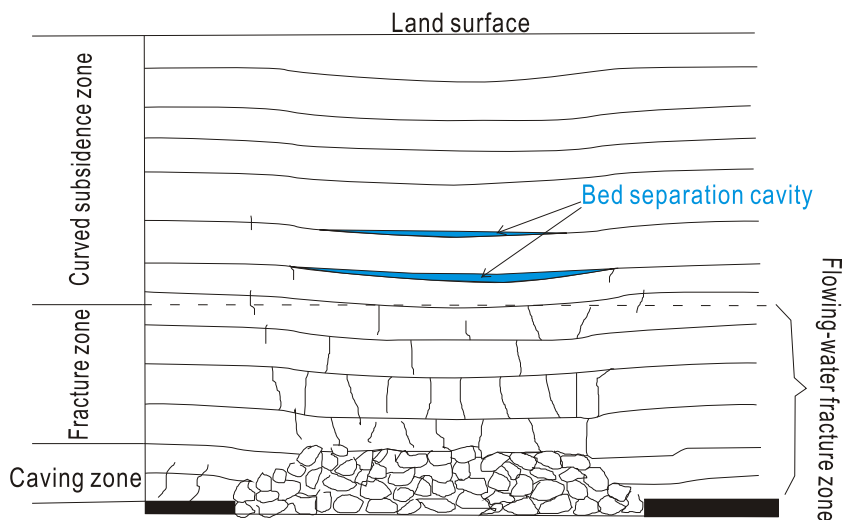
approximated to a rectangle; that is, only the red part, with length l_1, was included in the calculation. Therefore, the calculation model in Fig. 9a was simplified to a fixed beam with a length of l_1 and a uniform self-weight load of q_1. The load and bending moment distribution of the fixed beam are shown in Fig. 9b.

The curvature (C_1) of the first layer rock beam in the middle of its suspended span is calculated as:

$$(C_1) = C_1 = \frac{M_1}{E_1 I_1} \tag{7}$$

Fig. 9 TODA and TCM for one rock layer: (**a**) Range of TODA; (**b**) TCM and bending moment distribution

where M_1 is the bending moment of the beam, which is shown in Fig. 9b:

$$M_1 = \frac{q_1 l_1^2}{24} \tag{8}$$

At this point, it was also necessary to check whether the rock beam broke, i.e., whether the maximum tensile stress σ_{max1} on the rock beam exceeded its tensile strength σ_{s1}. The maximum tensile stress occurred at the position of maximum bending, i.e., at the ends of the rock beam (Fig. 9b). The maximum tensile stress is calculated as follows:

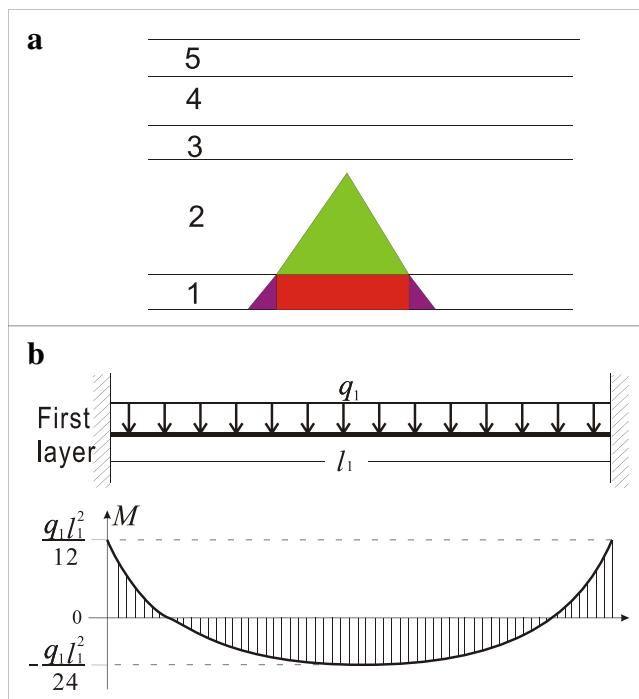$$\sigma_{\max1} = \frac{6M_1'}{h_1^2} \tag{9}$$

where M_1' is the bending moment of the first layer of the rock beam at its ends. The formula is:

$$M_1' = \frac{q_1 l_1^2}{12} \tag{10}$$

The calculation above is holds true only when $\sigma_{\max1} \leq \sigma_{s1}$.

$n = 2$

As shown in Fig. 10a, the first, second, and third rock layers were in the TODA, but only the first and second layers had their whole thicknesses within the TODA. To simplify the computational model, only the red portions of the first and the second layers were included in the calculation. The span lengths of the first and the second layers were l_1 and l_2, respectively, and the self-weight loads were q_1 and q_2, respectively. When the first and the second layers bended and sank simultaneously, the two rock beams came into contact and underwent squeezing. The load transmitted from one layer to

the other due to the contact extrusion between adjacent rock layers is called the contact load. The contact load between the first and second layers is written as $\Delta q_{(1, 2)}$. At this point, the computational model in Fig. 10a is reduced to two fixed beams, as shown in Fig. 10b.

The curvature (C_2) in the middle of the suspended span of a composite beam with two layers is calculated as follows:

$$(C_2) = (C_2)_1 = (C_2)_2 \tag{11}$$

where $(C_2)_1$ and $(C_2)_2$ are the curvatures of the first and second layers, respectively. The curvature is given by:

$$(C_2)_i = \frac{(M_2)_i}{E_i I_i}, (i = 1, 2) \tag{12}$$

where $(M_2)_i$ is the bending moment in the middle of the suspended span of the ith layer rock beam in the composite beam with two layers. According to the superposition theorem of the bending moment, the formula for $(M_2)_i$ can be obtained:

$$(M_2)_i = \begin{cases} \dfrac{l_1^2}{24}\left\{q_1 + \left[1 + \left(\alpha_{(1,2)}-1\right)^3\right]\Delta q_{(1,2)}\right\} , (i = 1) \\ \dfrac{l_2^2}{24}\left(q_2-\Delta q_{(1,2)}\right), \qquad\qquad\qquad (i = 2) \end{cases} \tag{13}$$

where $\alpha_{(1, 2)}$ is the ratio of the action length of contact load $\Delta q_{(1, 2)}$ to the action length of self-weight load q_1. The formula is:

$$\alpha_{(1,2)} = \frac{l_2}{l_1} \tag{14}$$

The above calculation is true only when the maximum tensile stress $\sigma_{\max\ i}$ of the ith layer rock beam and its tensile
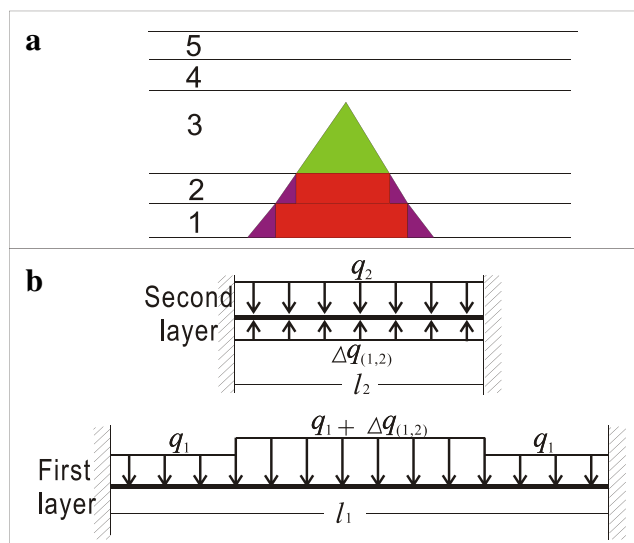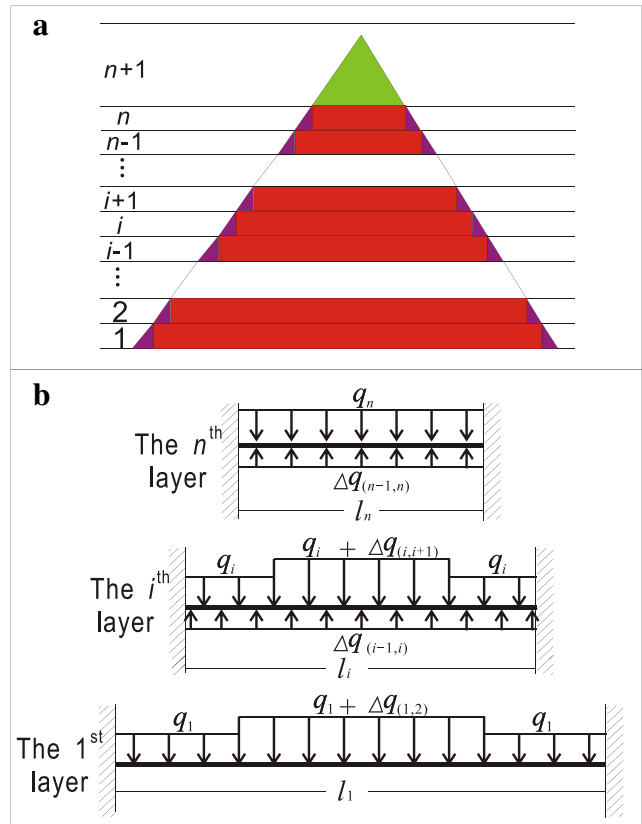
Fig. 11 TODA and TCM when the number of calculated rock layers is $n (n \geq 3)$: (**a**) TODA Range; (**b**) TCM

strength σ_{si} satisfy the condition $\sigma_{\max\ i} \leq \sigma_{s\ i}$. The maximum tensile stress occurs at the position of maximum bending, and the maximum tensile stress is calculated as:

$$\sigma_{\max i} = \frac{6(M_2)_i'}{h_i^2}, (i = 1, 2) \tag{15}$$

where $(M_2)_i'$ is the bending moment at both ends of the i-th layer rock beam in the composite beam with two layers. The formula is:

$$(M_2)_i' = \begin{cases} \dfrac{l_1^2}{24}\left[2q_1 + \left(3\alpha_{(1,2)}-\alpha_{(1,2)}^3\right)\Delta q_{(1,2)}\right], (i = 1) \\ \dfrac{l_2^2}{12}\left(q_2-\Delta q_{(1,2)}\right), \qquad\qquad\qquad (i = 2) \end{cases} \tag{16}$$

$n \geq 3$

As shown in Fig. 11a, only the 1st through n^{th} layers had their whole thicknesses within the TODA. To simplify the computational model, only these parts of these layers were included in the calculation. The span length of the ith layer was l_i, and the self-weight load was q_i. When these layers simultaneously bended and sank, any two adjacent rock beams in the

Fig. 10 TODA and TCM for two rock layers: (**a**) TODA Range; (**b**) TCM

composite beam came into contact and underwent squeezing. The contact load between the ith and $(i + 1)^{th}$ layers is written as $\Delta q_{(i , i + 1)}$. At this point, the computational model in Fig. 11a is reduced to n fixed beams in Fig. 11b.

The curvature (C_n) in the middle of the suspended span of the composite beam with n layers is calculated as follows:

$$(C_n) = (C_n)_1 = (C_n)_2 = ... = (C_n)_i = ... = (C_n)_{n-1}$$
$$= (C_n)_n \tag{17}$$

where $(C_n)_i$ is the curvature of the ith layer of rock beam in the composite beam with n layers. The formula is:

$$(C_n)_i = \frac{(M_n)_i}{E_i I_i}, (i = 1, 2...n) \tag{18}$$

$$(M_n)_i = \begin{cases} \frac{l_1^2}{24}\left\{q_1 + \left[1 + \left(\alpha_{(1,2)}-1\right)^3\right]\Delta q_{(1,2)}\right\}, & (i = 1) \\ \frac{l_i^2}{24}\left\{\left(q_i-\Delta q_{(i-1,i)}\right) + \left[1 + \left(\alpha_{(i,i+1)}-1\right)^3\right]\Delta q_{(i,i+1)}\right\}, & (2 \le i \le n-1) \\ \frac{l_n^2}{24}\left(q_n-\Delta q_{(n-1,n)}\right), & (i = n) \end{cases} \tag{19}$$

where $\alpha_{(i , i + 1)}$ is the ratio of the action length of the contact load $\Delta q_{(i , i + 1)}$ to the action length of self-weight load q_i. The formula is:

$$\alpha_{(i,i+1)} = \frac{l_{i+1}}{l_i} \tag{20}$$

The above calculations are true only when the maximum tensile stress $\sigma_{max\ i}$ of the ith layer rock beam and its tensile strength σ_{si} satisfy the condition $\sigma_{max\ i} \le \sigma_{s\ i}$. The maximum

where $(M_n)_i$ is the bending moment in the middle of the suspended span of the ith layer rock beam in a composite beam with n layers. Based on the position of the rock beam in the composite beam, there are three kinds of loads. The formulas for the bending moment of the rock layer vary for layers in the bottom, middle, and top portions. Thus, they should be analyzed and calculated separately. Based on the superposition theorem of the bending moment, the formulas of $(M_n)_1$, $(M_n)_i (2 \le i \le n-1)$, and $(M_n)_n$ can be obtained as:

tensile stress occurs at the position of maximum bending and is given by:

$$\sigma_{max i} = \frac{6(M_n)_i'}{h_i^2}, (i = 1, 2...n) \tag{21}$$

where $(M_n)_i'$ is the bending moment at both ends of the ith layer rock beam in the composite beam with n layers. The formula is:

$$(M_n)_i' = \begin{cases} \frac{l_1^2}{24}\left[2q_1 + \left(3\alpha_{(1,2)}-\alpha_{(1,2)}^3\right)\Delta q_{(1,2)}\right], & (i = 1) \\ \frac{l_i^2}{24}\left[2\left(q_i-\Delta q_{(i-1,i)}\right) + \left(3\alpha_{(i,i+1)}-\alpha_{(i,i+1)}^3\right)\Delta q_{(i,i+1)}\right], & (2 \le i \le n-1) \\ \frac{l_n^2}{12}\left(q_n-\Delta q_{(n-1,n)}\right), & (i = n) \end{cases} \tag{22}$$

A case study

Taking the overburden deformation and failure analysis of mining face 22302 in the Cuimu coal mine as an example, the application method of TCM was introduced. The mining face is located in the southwest portion of the Cuimu coal

mine (Fig. 2) and is 401-m long, 160-m wide, and 569.44-m deep . Table 2 lists the strata of the mining face overburden.

Table 2 shows that the Luohe Formation is composed of hard rock with a lithology of thick sandstone and conglomerate, while the Anding Formation is composed of soft rock with a lithology of mudstone and sandy mudstone. It is thus easy

Table 2 Strata characteristics and mechanical parameters of the overlying rock layer in mining face 22302

Stratigraphic position	Number of rock layer i	Lithology	Volume–weight γ_i (kN/m³)	Thickness h_i (m)	Accumulated burial depth H_i (m)	Elastic modulus E_i (GPa)	Tensile strength σ_s (kPa)
Quaternary series (Q)		Loess	14.7	97.15	97.15		
Cretaceous Luohe Formation (K_1l)	15	Fine sandstone	23.81	51.73	148.88	10.01	830
	14	Gravel sandstone	23.6	28.98	177.86	22.36	660
	13	Coarse sandstone	22.05	119.76	297.62	9.56	980
	12	Medium sandstone	23.13	14.16	311.78	9.27	1250
	11	Coarse sandstone	22.00	93.52	405.3	12.52	1180
Jurassic Anding group (J_2a)	10	Sandy mudstone	23.23	44.38	449.68	8.52	1380
	9	Mudstone	22.14	18.48	468.16	7.3	1210
	8	Sandy mudstone	23.34	52.08	520.24	9.41	1540
	7	Coarse sandstone	22.05	7.35	527.59	17.92	1650
Jurassic Zhiluo group (J_2z)	6	Siltstone	23.62	8.48	536.07	8.4	1560
	5	Fine sandstone	22.35	6.38	542.45	15.46	1088
Jurassic Yan'an Formation (J_2y)	4	Sandy mudstone	23.42	5.4	547.85	11.03	1850
	3	Mudstone	22.37	5.61	553.46	9.67	1250
	2	Coarse sandstone	22.75	10.6	564.06	25.84	3700
	1	Sandy mudstone	23.59	5.38	569.44	12.07	1973
		Mining seam	13.03	5.5	574.94	5.94	567

for bed separation to occur at the interface of the Luohe and Anding Formations during mining. The potential for BSWD occurs after water from the Luohe Formation aquifer accumulates in the bed separation cavity. In the early years, instances of BSWD occurred frequently during exploitation of mining faces 21301 and the 21302, and changes in the water level of the Luohe Formation aquifer before and after BSWD are shown in Fig. 12. Therefore, in the later period, analyzing the deformation of overburden and identifying the points of potential bed separation is necessary to prevent BSWDs during exploitation of the mining face.

Overburden deformation and breakage in FFZ

In previous operations at the Cuimu coal mine, the ratio of the height of the FFZ to mining seam thickness (RHT) at mining faces 21301 and 21302 was 21. Because mining faces 21301, 21302, and 22302 belong to the same mine field, geological conditions at both faces are similar, and the RHT of 22302 can also be taken as 21. The average mining thickness at 22302 was 5.5 m. The calculated FFZ above 22302 was 115.5 m. Table 2 indicates that the FFZ extended about 14.22 m into the 9th layer of rock, which had a thickness of 18.48 m, so the integrity of this layer had been destroyed, and the 9th layer of rock was placed in the FFZ. The analysis above shows that the 1st to the 9th layers were located in the FFZ, and the maximum height of the FFZ at 22302 was 119.76 m. After that, the deformation and breakage of the overburden in the FFZ were analyzed.

According to our calculations, when the advancing distance reached 36.21 m, $\sigma_{max\ 1}$ = 1973.14 kPa ≈ 1973 kPa = $\sigma_{s\ 1}$. This showed that the span length of the first layer reached its critical breaking length, and the first layer was broken if it continued to advance. The TODA of the first rock beam reaching the critical breaking distance is shown in Fig. 13. According to calculations, bed separations existed between the first and second layers and between the third and fourth layers. Moreover, because the fifth layer was not completely in the TODA, it did not undergo deformation or only a minimal amount. However, because of the bending subsidence of the fourth rock beam layer, there was also bed separation between the fourth and fifth layers. The analysis showed that there were three bed separations at this advancing distance, and the locations are shown in Table 3.

At this point, the first rock beam was separated from the rock beam above it. Thus, when the first rock beam had just broken, the upper strata did not break at once.

Similarly, in accordance with the above calculation principle, we inferred that the 2nd to the 5th layers of rock strata would break simultaneously when the excavation distance was 63.45 m. When the excavation distances reached 81.79 m and 89.98 m, the 6th and the 7th layers of rock strata would break, respectively. The 8th and 9th layers of rock strata would break simultaneously when the excavation distance reached 191.88 m. The distribution of bed separations at different critical breaking distances is shown in Table 4.
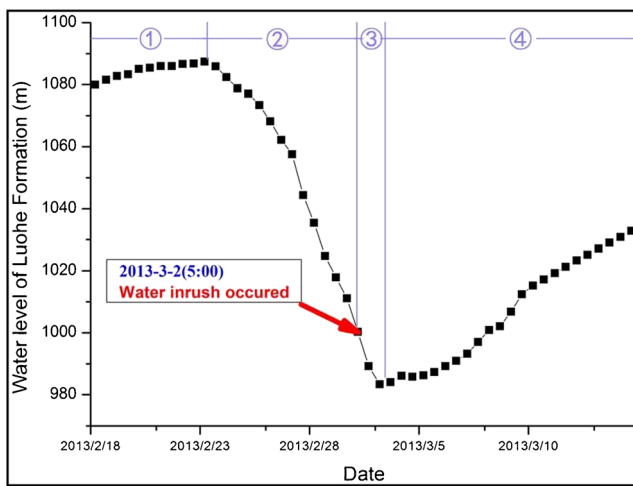
Fig. 12 Water level changes in the Luohe Formation aquifer before and after BSWD at mining face 21301, according to G1 drill hole (① refers to the natural recovery stage of the water level, ② refers to the water filling stage of the bed separation cavity, ③ refers to the water inrush stage during a BSWD, and ④ refers to the stage of water level recovery after closure of the fissure)

Overburden deformation in curved subsidence zone

It was found that when the excavation distance was 189.53 m, the TODA began to extend to the 11th layer of rock strata, at which time a bed separation between the 10th and the 11th layers appeared. If the 10th layer of rock was not contact with the 11th layer, then according to the calculation method in Overburden deformation and breakage in FFZ, the 11th and 12th layers broke simultaneously (because of the contact between these strata and

the calculated $\Delta q_{(11,\ 12)}$ = 318.56 kPa) when the excavation distance was 391 m. In fact, the 11th and 12th layers were located in the curved subsidence zone, which were supported by the lower strata before reaching the critical breaking distance and did not break. Therefore, we concluded that when the excavation distance was 189.53–391 m, there was bed separation between the 10th and the 11th layers, and when the excavation distance reached around 391 m or the excavation distance exceeded 391 m, the water in the bed separation cavity was squeezed by the 11th layer of rock. This squeezing may have driven the water accumulated in the bed separation between the 10th and the 11th layers out of the bed separation cavity to the mining face by breaking through the 10th layer because this separation was not far from the FFZ, causing a BSWD accident like the one that occurred at mining face 21301.

Because the position with an excavation distance of 391 m was only 10 m away from the stopping line (i.e., excavation distance 401 m), when the excavation distance was 391–401 m, detailed calculation and analysis of overburden deformation were not carried out.

Validation

Based on the calculations and analysis in Overburden deformation in curved subsidence zone, we have drawn the following inferences:
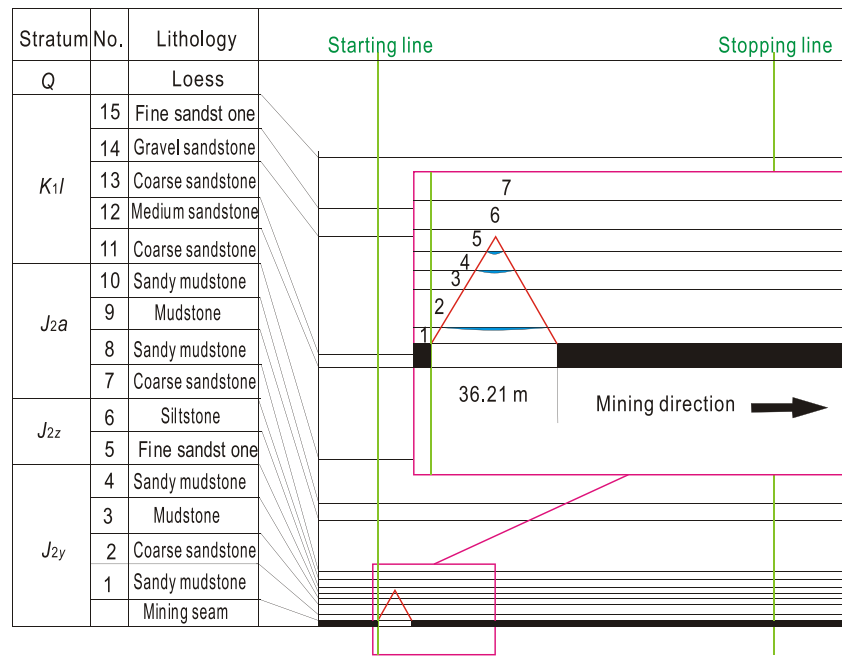
(1) When the excavation distance was greater than 191.88 m, the FFZ expanded into the 9th layer of rock, at which

Table 3 Bed separation locations when the first rock beam reached its critical breaking distance[*]

Number of rock layer i	Span length l_i (m)	Curvature $(C_n)_i$ $(1 \times 10^{-6} \cdot \mathrm{m}^{-1})$		Maximum tensile stress $\sigma_{\max\ i}$ (kPa)	Tensile strength $\sigma_{s\ i}$ (kPa)	Was there a bed separation above this layer?
		HierarchyI	HierarchyII			
15	--	--	--	--	--	N
14	--	--	--	--	--	N
13	--	--	--	--	--	N
12	--	--	--	--	--	N
11	--	--	--	--	--	N
10	--	--	--	--	--	N
9	--	--	--	--	--	N
8	--	--	--	--	--	N
7	--	--	--	--	--	N
6	--	--	--	--	--	N
5	-	-	-	-	-	N
4	5.05	0.93	0.93	55.22	1850	Y
3	11.285	4.68	1.63	88.64	1250	Y
2	17.76	1.24	1.63	433.00	3700	N
1	30.00	30.39	30.39	1973.14	1973	Y

([*] "--" indicates that the rock layer is not in the TODA; "-" indicates that only a part of this rock layer is in the TODA)

Fig. 13 The TODA and the distribution of bed separations when the first rock beam reached its critical breaking distance

(2) point the height of the FFZ no longer increased with excavation distance.

(2) When the excavation distance was 189.53–391 m, there was bed separation between the 10th and 11th layers that was compacted closed when distance reached around 391 m or exceeded 391 m.

To validate the inferences above, we needed to obtain the development of fissures in overlying rocks; thus, we conducted television imaging observations (TIO) in drill holes. When the excavation distance reached 290 m and 400 m, TIO in drill hole X22302 was carried out. Images from depths of 405 m (the interface between the 11th rock layer and the 10th layer), 448 m (i.e., the bottom of the 10th rock layer) and 458 m (the upper part of the 9th rock layer) are shown in Fig. 14.

Through the observation and analysis of the images obtained from TIO, we validated the above inferences as follows:

Table 4 Distribution of bed separations at different critical breaking distances[*]

Number of rock layer i	Was there a bed separation above this layer at different critical breaking distances?				
	36.21 m	63.45 m	81.79 m	89.98 m	191.88 m
15	--	--	--	--	--
14	--	--	--	--	--
13	--	--	--	--	--
12	--	--	--	--	--
11	--	--	--	--	-
10	--	--	--	--	Y
9	--	--	--	--	Y
8	--	-	-	-	N
7	--	Y	Y	Y	\
6	--	Y	Y	\	\
5	-	Y	\	\	\
4	Y	Y	\	\	\
3	Y	N	\	\	\
2	N	N	\	\	\
1	Y	\	\	\	\

([*] "–" indicates that the rock layer is not in the TODA; "-" indicates that only a part of this rock layer is in the TODA; "\" indicates that the rock layer has been broken)

Fig. 14 Drill hole TV images of the X22302 at different depths and excavation distances: (**a**) Depth 405 m, footage of 290 m; (**b**) Depth 405 m, footage of 400 m; (**c**) Depth 448 m, footage of 290 m; (**d**) Depth 448 m, footage of 400 m; (**e**) Depth 458 m, footage of 290 m; (**f**) Depth 458 m, footage of 400 m
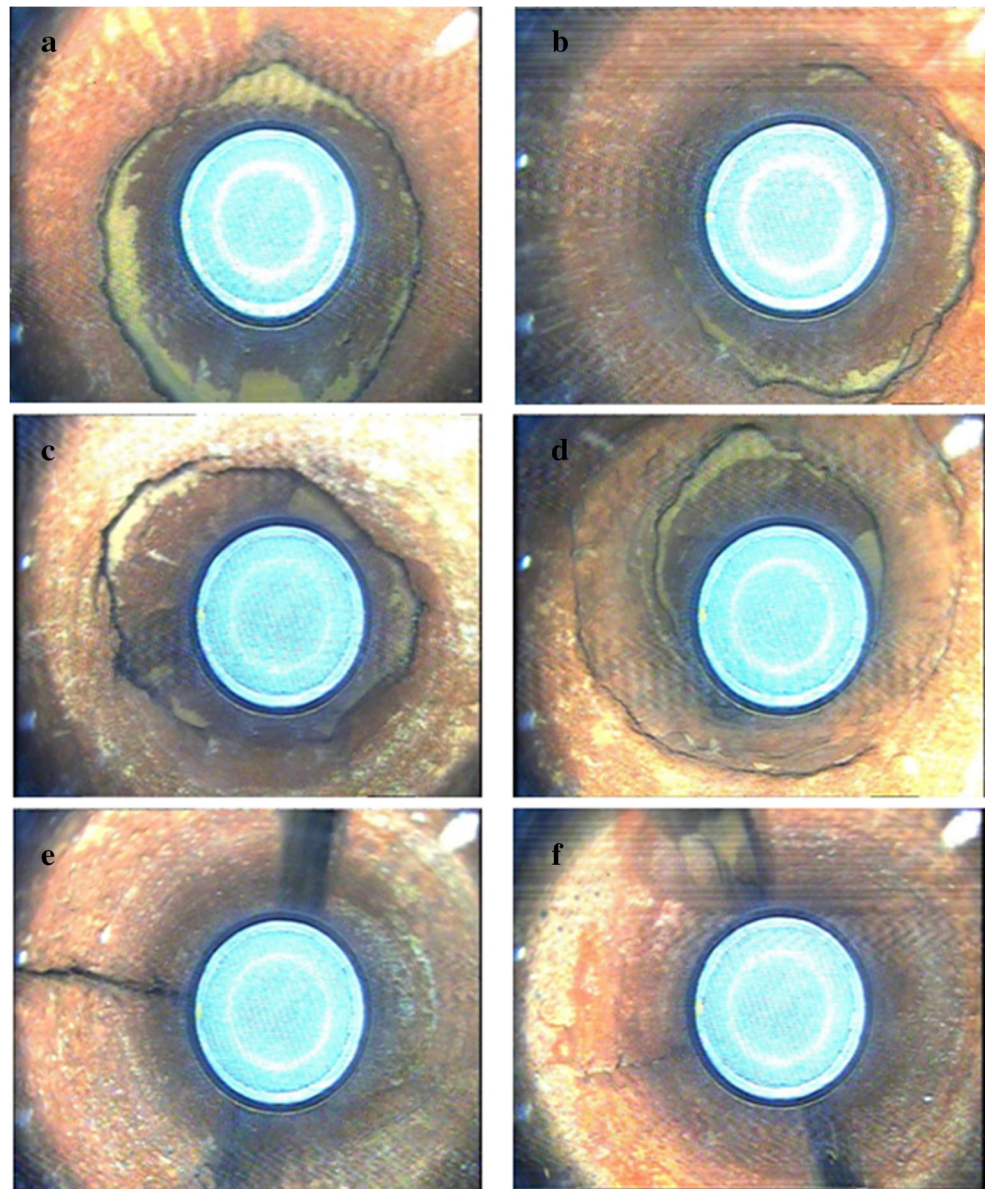
(1) Figure 14 shows that when the excavation distance reached 290 m, the area of vertical fractures (i.e., FFZ) extended into the 9th layer of rock, and no vertical fractures were observed in the 10th to 11th layers, only horizontal fissures. When the excavation distance reached 400 m, there were still no vertical fractures in the 10th to the 11th layers, but the shape of the previous horizontal fissures changed due to the disturbance of mining and the erosion of water flow. Therefore, after expanding into the 9th layer of rock, the FFZ no longer extended upward.

(2) Comparison with Fig. 14a and b shows that when the excavation distance reached 290 m, a large horizontal gap (i.e., bed separation) occurred at the contact of the 11th and the 10th layers, and then, the bed separation was compacted closed due to the sinking and squeezing of the 11th layer of rock when the excavation distance reached 400 m. Comparison with Fig. 14e and f shows that when the excavation distance reached 400 m, the vertical fractures were squeezed by the upper strata so that their crack width was reduced, and some small rock particles were taken into the vertical fractures under the action of running water.

Conclusions

Based on pressure arch theory, composite beam theory, similar simulation experiments, and field measurements, a

modeling approach was considered to predict bed separation position, coal roof collapse, and catastrophic water inflows during underground coal mining. This calculation model was derived as follows.

First, the concept of a triangular overburden deformation area (TODA) was proposed to determine the shape of the overburden deformation area based on the results of similar material simulation experiments. Then, a hierarchy comparison merging method (HCMM) based on the principle of a composite beam was used to distinguish the contact state between strata. The acquisition of the contact state of each rock layer provided a basis for the calculation of the actual load of each rock layer when judging its failure state. Finally, a triangular calculation model (TCM) that could be used to identify bed separation positions and analyze overburden breakage was established by combining the TODA with HCMM. The instructions for using the model and the related formulas were described, and the model was applied and validated in a mining case.

Simplifying the shape of the overburden deformation area into a triangle and using HCMM to identify the bed separation position were the two innovative points of this study. The calculation model provides a practical tool for identifying bed separation positions, and calculating the excavation distance when overburden is broken. The research results can provide useful guidance for the prevention of BSWD. It is suggested to dredge the bed separation water in advance after identifying the position of a hidden BSWD danger and to add drainage facilities at the excavation distance where the overburden breakage and BSWD are expected to occur, to ensure coal mining safety.

References

An ZH, Wu LF (2008) Roadway roof separation mode and main influencing factor. Coal Sci Technol Mag 01:16–18

Bieniawski ZT (1990) Strata control in mineral engineering. China University of Mining and Technology Press, Xuzhou

Chai J, Liu JC, Qiu B, Li Y, Zhu L, Wei SM, Wang ZP, Zhang GW, Yang JH (2011) Detecting deformations in uncompacted strata by fiber Bragg grating sensors incorporated into GFRP. Tunn Undergr Space Technol 26(1):92–99

Chai J, Wang S, Yuan Q, Jiang DJ, Li Y (2015) Experimental study on the separation evolution of overlying strata above the stope by FBG sensing. J Xian Univ Sci Technol 35(02):144–151

Cheng GW, Ma TH, Tang CA, Liu HY, Wang SJ (2017a) A zoning model for coal mining-induced strata movement based on microseismic monitoring. Int. J. Rock. Mech Min Sci 94:123–138

Cheng JW, Zhao G, Li SY (2017b) Predicting underground strata movements model with considering key strata effects. Geotech Geol Eng 36:621–640. https://doi.org/10.1007/s10706-017-0307-8

Ding EJ, Zhao ZP, Miao SG, Yu NN (2010) Design of coalmine roadway abscission layer monitoring system based on WSNS. Transducer Microsyst Technol 29(04):108–110

Fan J (2014) Roof abscission layer wireless monitoring network system. Ph.D. Thesis, Taiyuan University of Technology

Gao YF (1996) Four-zone model of rock mass movement and back analysis of dynamic displacement. J China Coal Soc 21(1):51–55

Gao YF, Deng ZY, Yang ZD, Li WC, Xie HR (2001) Theoretical study of subsidence reduction by grouting in overlying rock separation zone. Ground Press Strata Control 4:65–67

He JH, Li WP, Liu Y, Yang Z, Liu SL, Li LF (2018) An improved method for determining the position of overlying separated strata in mining. Eng Fail Anal 83:17–29

Jiang Y (1997) Bed-separated zone and its distribution law in the overlying strata affected by mining. J Shandong Min Inst 16(1):19–23

Jiang Y, Xu YM (1997) Calculation of overburden strata separation in mining. Coal Min Technol 26(3):41–42

Kuang TJ, Li Z, Zhu WB, Xie JL, Ju JF, Liu JR, Xu JM (2019) The impact of key strata movement on ground pressure behaviour in the Datong coalfield. Int J Rock Mech Min Sci 119:193–204

Liu TQ (1981) Law and application of surface movement and overlying rock failure in coal mine. Coal Industry Press, Beijing

Liu XS, Tan YL, Ning JG, Tian CL, Wang J (2015) The height of water-conducting fractured zones in longwall mining of shallow coal seams. Geotech Geol Eng 33:693–700

Lu CP, Liu Y, Wang HY, Liu PF (2016) Microseismic signals of double-layer hard and thick igneous strata separation and fracturing. Int J Coal Geol 160–161:28–41

Man XL (2014) Study on evolution law of allometric growth of mining overburden separated strata. Ph.D. Thesis, Qingdao Technological University

Palchik V (2003) Formation of fractured zone in overburden due to longwall mining. Environ Geol 44(1):28–38

Palchik V (2005) Localization of mining-induced horizontal fractures along rock layer interfaces in overburden: field measurements and prediction. Environ Geol 48(1):68–80

Palchik V (2010) Experimental investigation of apertures of mining-induced horizontal fractures. Int J Rock Mech Min Sci 47(3):502–508

Peng SS (1984) Coal mine ground control. Coal Industry Press, Beijing

Qian MG, Shi PW (2003) Mine pressure and strata control. China University of Mining and Technology Press, Xuzhou

Qian MG, Miao XX, Xu JL, Mao XB (2003) Key stratum theory of strata control. China University of Mining and Technology Press, Xuzhou

Qiao W, Li WP, Li T, Chang JY, Wang QQ (2017) Effects of coal mining on shallow water resources in semiarid regions: a case study in the Shennan Mining Area, Shaanxi, China. Mine Water Environ 36: 104–113

Su ZJ (2001) Research of deformation mechanism of mining overburden separated strata. Ph.D. Thesis, Liaoning Technology University

Su ZJ, Yu GM, Yang L (2003) Numerical simulation on mechanism of deformation of separated strata in overburden. Chin J Rock Mech Eng 22(08):1287–1290

Sun ZG (2012) Movement law of overlying rock in large mining height face by simulation. J Liaoning Technol Univ (Natural Science) 31(02):181–184

Tan YL, Yu FH, Chen L (2013) A new approach for predicting bedding separation of roof strata in underground coalmines. Int J Rock Mech Min Sci 61:183–188

Wang SF, Li XB (2016) Dynamic distribution of longwall mining-induced voids in overlying strata of a coalbed. Int J Geomech 17(6):04016124

Wang JZ, Kang JR, Wu LX (1999) Discussion on mechanism and application of grouting in separated-bed to reduce surface subsidence induced by coal mining. J China Univ Min Technol 28(04):331–334

Wang LX (2013) Building the geological model to forecast inrush of bed separation water in overlying strata due to coal mining and its application. Ph.M. Thesis, China University of Mining & Technology

Wang C, Zhang NC, Han YF, Xiong ZQ, Qian DY (2015) Experiment research on overburden mining-induced fracture evolution and its fractal characteristics in ascending mining. Arab J Geosci 8:13–21

Wang SF, Li XB, Wang DM (2016a) Void fraction distribution in overburden disturbed by longwall mining of coal. Environ Earth Sci 75(2):151

Wang SF, Li XB, Wang DM (2016b) Mining-induced void distribution and application in the hydro-thermal investigation and control of an underground coal fire: A case study. Process Saf Environ Prot 102: 734–756

Wang SF, Li XB, Wang DM (2017) Separation and fracturing in overlying strata disturbed by longwall mining in a mineral deposit seam. Eng Geol 226:257–266

Wei JC, Wu FZ, Yin HY, Guo JB, Xie DL, Xiao LL, Zhi H, Lefticariu L (2017) Formation and height of the interconnected fractures zone after extraction of thick coal seams with weak overburden in western China. Mine Water Environ 36:59–66

Wen ZM, Zhang HW (2006) Roof abscission layer and monitor. Coal Technol 25(03):49–51

Wu DY, Gao H, Wang AL (2012) Sensitivity analysis of influence factors on interlayer separation of complex roof. J Min Saf Eng 29(02):255–260

Xiao F, Zhang CS, Ni JM, Chen G, Liu WG, Li C (2015) Regression analysis and stability evaluation of the coal mine gateway roof abscission layer. Opt Technol 41(03):243–246

Xu JL, Qian MG, Jin HW (2004) Study and application of bed separation distribution and development in the process of strata movement. Chin J Geotech Eng 24(5):632–636

Xu C, Cheng YP, Ren T, Wang L, Kong SL, Lu SQ (2014) Gas ejection accident analysis in bed splitting under igneous sills and the associated control technologies: a case study in the Yangliu Mine, Huaibei Coalfield, China. Nat Hazards 71:109–134

Xu T, Yang TH, Chen CF, Liu HL, Yu QL (2015) Mining induced strata movement and roof behavior in underground coal mine. Geomech Geophys Geo-Energ Geo-Resour 1:79–89

Xue JH, Wang HP, Zhou W, Ren B, Duan CR, Deng DS (2015) Experimental research on overlying strata movement and fracture evolution in pillarless stress-relief mining. Int J Coal Sci Technol 2(1):38–45

Yan H, He FL, Yang T, Li YY, Zhang SB, Zhang JX (2016) The mechanism of bedding separation in roof strata overlying a roadway within a thick coal seam: a case study from the Pingshuo Coal, China. Eng Fail Anal 62:75–92

Yu T (2007) Numerical simulation study on solidify effect of overburden separated grouting. Ph.D. Thesis, Liaoning Technology University

Yu T, Wang LG (2006) Mechanism of generation of overburden separate layer. J Liaoning Technol Univ 25(Suppl):132–134

Yue JG, Yang WF, Gu CS (2015) Formation mechanism and identification method of super-high seam by fully mechanized caving method. J Eng Geol 23(Suppl):603–610

Zhang YZ, Chen LL (1996) Conditions for bed separation of overlying burden in longwall mining. J China Coal Soc 21(06):576–581

Zhang D, Wang JC, Zhang PS, Shi B (2017) Internal strain monitoring for coal mining similarity model based on distributed fiber optical sensing. Measurement 97:234–241

Zhao Q (2016) Development of mining roadway roof abscission layer monitoring system based on mesh network transmission. Ph.D. Thesis, Taiyuan University of Technology

Zhao DS, Fan XL, Liu WS, Sun QH, Wang SP (1998) Analysis of the effect of geologic and mining factors on the law of separated strata distribution. J Liaoning Technol Univ (Natural Science) 17(02): 119–123

Zhao DS, Zhu GY, Liu WS, Fan XL (2002) Test study on the space-time laws of overburden separated layer. J Liaoning Technol Univ (Natural Science) 21(01):4–7

Zhao TZ, Li WP, Zhao CX, Li XQ, Sun RH (2008) Investigation of water distribution law of overlying strata separation. Min Saf Environ Prot 35(05):4–6

Zhao ZG, Zhang YJ, Li C, Zhou W, Li YN, Wang K, Xu JF (2015) Monitoring of coal mine roadway roof separation based on fiber bragg grating displacement sensors. Int J Rock Mech Min Sci 74: 128–132

Zhou DK (2015a) Formation and prevention of water inrush from bed separation in cuimu coalmine. Ph.M. Thesis, China University of Mining & Technology

Zhou FF (2015b) Roof separation measure and separate interlayer in KouZiDong mine. Ph.D. Thesis, Anhui Jianzhu University